Nanoprotonics in perovsikte-type oxides : Reversible changes in color and ion conductivity due to nanoionics phenomenon in platinum-containing perovskite oxide

Matsumoto, Hiroshige
INAMORI Frontier Center, Kyushu University

Tanji, Takayoshi
EcoTopia Science Institute, Nagoya University

Amezawa, Koji
Graduate School of Environmental Studies, Tohoku University

Kawada, Tatsuya
Graduate School of Environmental Studies, Tohoku University

他

出版情報：Solid State Ionics. 182 (1), pp.13-18, 2011-02-03. Elsevier
バージョン：

Nanoprotonics in perovsikte-type oxides: Reversible changes in color and ion conductivity due to nanoionics phenomenon in platinum-containing perovskite oxide

Hiroshige Matsumoto[1*], Takayoshi Tanji[2], Koji Amezawa[3], Tatsuya Kawada[3], Yoshiharu Uchimoto[4], Yoshihisa Furuya[5], Takaaki Sakai[1], Maki Matsuka[5] and Tatsumi Ishihara[2]

[1]INAMORI Frontier Center, Kyushu University, Nishi-ku, Fukuoka 819-0395, Japan
[2]EcoTopia Science Institute, Nagoya University, Furo-cho, Chikusa-ku, Nagoya 464-8603, Japan
[3]Graduate School of Environmental Studies, Tohoku University, Aoba-ku, Sendai 980-8579, Japan
[4]Graduate School of Human and Environmental Studies, Kyoto University, Sakyo-ku, Kyoto 606-8501, Japan
[5]Department of Applied Chemistry, Faculty of Engineering, Kyushu University, Nishi-ku, Fukuoka 819-0395, Japan

Abstract

The ion conductivity of a solid-state material is primarily a function of its chemical composition and crystal structure. However, interfaces can play an important role in the conduction process. The effects of interfaces on ionic properties can be controlled on the basis of "nanoionics". In this study, we demonstrate a nanoionics phenomenon observed in a blue platinum-containing perovskite. The proton conductivity changed reversibly in response to the precipitation of platinum nanoparticles and oxidation to form a solid solution. The results of XAFS measurements, TEM analysis, and electron holography provide evidence of the nanoionics phenomenon, and suggest a possible underlying mechanism for the conductivity change caused by the small amount of precipitated platinum nanoparticles in the perovskite oxide.

Keywords: nanoprotonics, proton conductor, perovskite, platinum nanoparticle, space charge.

[*]Corresponding author: Hiroshige MATSUMOTO
Environmental Technology Research Division, INAMORI Frontier Research Center, Kyushu University
744 Motooka, Nishi-ku, Fukuoka 819-0395, Japan, Tel: +81-92-802-6964, Fax: +81-92-802-6964, E-mail: matsumoto@ifrc.kyushu-u.ac.jp

1. Introduction

Ion conduction in solid-state materials occurs via point defects [1-2]. When designing ion conductors, it is important that their compositions and crystal structures be designed to introduce ionic defects that can serve as charge carriers, and to increase the concentration and mobility of these charge carriers. Although the ion conductivity of a solid-state material is generally determined by its chemical composition and crystal structure, interfaces in the solid structure also play an important role in ion conduction [3]. A grain boundary is a homo-interface and is important for polycrystalline materials. The contribution of interfaces to the ionic properties of solid-state materials can be controlled on the basis of "nanoionics" [4-6], and a few experiments have been previously reported in this area [7-9].

Solids with a secondary phase, that is, composites, contain hetero-interfaces, leading to greater variation in the ionic properties of such materials. The work functions of the two phases differ; thus, charge transfer occurs at the junction of the two phases, resulting in the formation of an electrically charged zone, referred to as a space charge layer [3-4, 6]. Ionic carriers are electrically charged in the layer, and increase or decrease due to the influence from the space charges. The charged layer decays over a distance in relation to the Debye length, which is a distance over which the electric field of an ion is screened by other nearby ions. The effective thickness of the space charge can be assumed as twice to several times the Debye length, and is typically of the order of one to several tens of nanometers. Therefore, nanostructured composites of ion-conducting solids containing many hetero-interfaces could possibly exhibit a more noticeable nanoionics effect.

Proton-conducting oxides, currently attracting much attention for energy applications [10-11], contain protonic charge carriers that originate from the dissolution of ambient water molecules into the oxide ion vacancies in their crystal lattices [12-14]. Protons in the oxides are in equilibrium with holes and electrons, and the oxides are expected to have different characteristics at hetero-interfaces where space charges are generated and affect these defect equilibria.

In our previous studies [15-16], a decrease in the electrical conductivity of oxide samples was observed upon the introduction of the platinum phase, which was probably due to the nanoionics effect. However, the sample contained many micrometer-sized platinum particles; thus, the phenomenon could not be fully attributed to the nanoionics effect. In this study, we aimed to

examine the effects of finely and homogeneously dispersed platinum nanoparticles in perovskite oxides, and thereby to demonstrate the nanoionics phenomenon. In this study, a platinum-containing proton-conducting oxide (composite) was examined, namely, $SrZr_{0.9}Y_{0.1}O_{3-\alpha}$. To avoid the formation of coarse platinum grains and to fully incorporate the platinum nanoparticles into the oxides, citric acid-combustion synthesis using a thermally stable platinum complex ($[Pt(NH_3)_4](NO_3)_2$) was employed in this study. The ratio of platinum metal to the oxide was as low as 0.5 vol %. Sintering temperatures were also examined to find the optimal temperature for forming a solid solution of platinum in the perovskite lattice.

2. Experimental

$SrZr_{0.9}Y_{0.1}O_{3-\alpha}$ and Pt-containing $SrZr_{0.9}Y_{0.1}O_{3-\alpha}$ were prepared from an aqueous solution of strontium nitrate, oxyzirconium nitrate, yttrium nitrate, and tetraammine platinum (II) nitrate. The solution also contained EDTA, citric acid, and ammonium nitrate for polymerization and combustion. The solution was heated with stirring until ignition occurred. The resulting powder was heat-treated at 700 °C in air, ball-milled, pressed into pellets and sintered at a given temperature for 10 h in air.

The sintered samples were cut into rectangular bars (typically, 3 mm × 3 mm × 15 mm) for the electrical conductivity measurement. Pt paste was applied to the bars, and fired at 950 °C for 15 min in air to form porous Pt electrodes for either applying a current or sensing the voltage. The conductivity was measured by the dc four-probe method in humidified H_2 or O_2 (saturated with water vapor at 17.0 °C: $p(H_2O)$ = 1.9 kPa) at 1000 °C.

X-ray absorption fine structure (XAFS) spectra at the Pt L_{III}-edge (11.56 keV) were obtained at beamline BL-7C of the 2.5 GeV storage ring at Photon Factory, High Energy Accelerator Research Organization, KEK, in Tsukuba, Japan. The X-ray beam was monochromatized with a Si(111) double-crystal monochromator. Absorption spectra were collected in transmission mode at room temperature. Transmission electron microscopy (TEM) and electron holography analyses were performed at an acceleration voltage of 200 kV (Hitachi HF-2000 FE-TEM). The phases of electron waves were reconstructed such that the larger values corresponded to the lower electrostatic potentials, which were higher in electron energy. The spatial resolution of TEM was less than 0.2 nm, and that of electron holography was less than 2 nm. The thickness of the samples was controlled by conventional mechanical polishing and ion milling.

3. Results and discussion

3.1 Synthesis and electrical conductivity of $SrZr_{0.9}Y_{0.1}O_{3-\alpha}$ and Pt-containing $SrZr_{0.9}Y_{0.1}O_{3-\alpha}$

Figure 1shows (A) the appearance $SrZr_{0.9}Y_{0.1}O_{3-\alpha}$ (platinum free, sintered at 1600 °C), (B) the appearance of Pt-containing $SrZr_{0.9}Y_{0.1}O_{3-\alpha}$ (sintered at 1350 °C), and (C) the XRD patterns of Pt-containing $SrZr_{0.9}Y_{0.1}O_{3-\alpha}$ sintered at different temperatures and the corresponding appearance of the specimen. Peaks marked with a circle and with triangles in Figure 1 (C) are assigned to the reflections from the $SrZrO_3$ phase and metallic platinum, respectively; the two platinum peaks are due to Cu-Kα_1 and Cu-Kα_2 splitting.

The sintered $SrZr_{0.9}Y_{0.1}O_{3-\alpha}$ was originally light brown as shown in Figure 1 (A). In order to introduce platinum as nanoparticles, citric acid-combustion synthesis using thermally stable platinum complex ($[Pt(NH_3)_4](NO_3)_2$) was employed in this study, and different final sintering temperatures were also examined. The ratio of platinum metal to the oxide was as low as 0.5 vol %. As a result, a blue specimen of Pt-containing $SrZr_{0.9}Y_{0.1}O_{3-\alpha}$ was obtained (Figure 1 (B)). As shown in Figure 1 (C), there were notable differences in color among the Pt-containing $SrZr_{0.9}Y_{0.1}O_{3-\alpha}$ specimens sintered at different temperatures. As shown in Figure 1 (C), no metallic platinum phase was detected in the blue oxide specimens by XRD analysis. This possibly indicates that the introduced platinum was in solid solution in the oxide, provided that the platinum was substituted into the *B*-site of the ABO_3 perovskite structure and the amount of platinum corresponded to 1 mol % of the *B* site. As the final sintering temperature was increased, the color of the specimen changed from blue to black, and metallic platinum peaks started to appear in the corresponding XRD pattern. The final sintering temperature of 1350 °C was optimal for the complete solid dissolution of the platinum with the highest relative density of 70.1%.

Figure 2 shows the electrical conductivity of $SrZr_{0.9}Y_{0.1}O_{3-\alpha}$ and Pt-containing $SrZr_{0.9}Y_{0.1}O_{3-\alpha}$ measured at 1000 °C in a series of different ambient atmospheres. Both specimens were prepared by the same procedure and sintered at 1350 °C. The relative density of $SrZr_{0.9}Y_{0.1}O_{3-\alpha}$ was 59.8%, and that of Pt-containing $SrZr_{0.9}Y_{0.1}O_{3-\alpha}$ was 70.1%. The conductivity was corrected to the full-density conductivity using an empirical equation: $\sigma_d = 2(0.01r_d - 0.5) \times \sigma_r$, where σ_d, σ_r, and r_d are the measured conductivity, full-density conductivity, and relative density, respectively [17]. The ambient atmosphere was changed in the order of (1) O_2 → (2) Ar → (3) H_2 → (4) Ar → (5)

O_2.

In O_2 and Ar atmospheres, the conductivity of the blue Pt-containing specimen was similar to that of the Pt-free one. Both specimens exhibited typical trends in conductivity with respect the change of the surrounding atmosphere; that is, the conductivity was higher in O_2 and in Ar, owing to hole conductivity. However, when the atmosphere was changed to hydrogen gas, the conductivity of the Pt-containing specimen decreased markedly; the response was high because of the porosity of the specimen, which allowed easy access of the hydrogen gas to the interior of the specimen. This indicates that the introduction of platinum had an effect that led to the decrease in conductivity.

The inset photographs in Figure 2 show the appearance of Pt-containing specimens quenched at different stages of the conductivity measurement. The color of the specimen was blue at the beginning of the conductivity measurement. At stage (3), the specimen was quenched, and the color turned from blue to black. During subsequent changes of atmosphere, (3) H_2 → (4) Ar → (5) O_2, the reduced conductivity returned approximately to the initial values in Ar and O_2, and more importantly, the color of the specimen returned to blue. Interestingly, the color of the Pt-containing perovskite changed between black in H_2 atmosphere and blue in O_2 atmosphere, and the conductivity decreased and recovered again, both in a reversible manner.

3.2 Characterization of Pt-containing blue and black specimens

Figure 3 shows results of XAFS measurements and TEM images of as-prepared (blue) and hydrogen-treated (black) Pt-containing specimens. Figure 3 (A) shows the normalized Pt L_{III}-edge XANES spectra, and Figure 3 (B) shows the radial structural functions around a platinum atom obtained from the Pt L_{III}-edge EXAFS oscillation. The gray dotted curves in Figure 3 (A) and 3 (B) show the data for a platinum metal foil as reference. The XANES spectrum of the hydrogen-treated black specimen (black line) is similar to that of the reference, indicating a metallic state of platinum in the specimen. The spectrum of the as-prepared blue specimen (blue line) apparently differs from the other two spectra. The XAFS measurement of the blue and black specimens (Figure 3 (A) and 3 (B)) reveals that the blue perovskite contained oxidized platinum, which formed Pt-O bonds (peak at around 1.65 Å in Figure 3 (B)), and that the black specimen contained metallic platinum with Pt-Pt coordination (2.66 Å).

TEM images of the as-prepared (blue) and hydrogen-treated (black) Pt-containing samples,

respectively, are shown in Figure 3 (C) and 3 (D). Homogeneous nanoparticles of 1-3 nm in diameter are apparent in the hydrogen-treated black sample (Figure 3 (D)), whereas the blue specimen did not contain such particles ((C)). The typical grain size of strontium zirconate oxide is ~1 μm, which is much larger than the scale shown in the figures; in other words, the platinum particles precipitated in the grain interior of the oxide. These results clearly demonstrate that the above-mentioned changes in conductivity are due to the precipitation of the platinum nanoparticles. The electrical properties of the as-prepared blue perovskite were not drastically affected by the introduction of platinum, as the platinum was still dissolved in the oxide as cations via the formation of a solid solution, which does not strongly affect the defect equilibrium. The decrease in conductivity was observed only when the platinum nanoparticles precipitated in the system, as in the black hydrogen-treated specimen. These results also show that the precipitated platinum uniformly takes the form of nanoparticles; otherwise, coarse platinum particles would have been detected by the XAFS measurements.

The XRD patterns of as-prepared and hydrogen-treated (at 1000 °C) Pt-containing $SrZr_{0.9}Y_{0.1}O_{3-\alpha}$ samples are shown in Figure 4 (A). It should be noted that the specimens were sintered at 1350 °C; that is, the pattern of the as-prepared sample (blue line) is the same as the one (1350 °C) in Figure 1 (C). In both as-prepared and hydrogen-treated samples (Figure 4 (A)), only the peak at around $2\theta = 39.5\text{-}39.7°$, which corresponds to the reflection from the (131) plane of orthorhombic (Pnma) $SrZrO_3$ perovskite, can be identified, while no peak at 39.8°, which corresponds to the (111) reflection of platinum, was detected. The absence of the platinum peak suggests that no large platinum particles were present in the hydrogen-treated specimen.

By examining the patterns more closely, it can be seen that there is a small hump at around 40° in the hydrogen-treated specimen. Figure 4 (C) shows Lorenz curves, and two peaks, namely, Peak 1 from perovskite and Peak 2 from platinum, fit the pattern, suggesting that small platinum particles formed in the hydrogen-treated specimen. In the case of the as-prepared specimen (Figure 4 (B)), only one Lorentz curve (Peak 1) matches the XRD pattern.

The XRD analysis suggests that no large platinum grains were present in the specimens. Such precipitation of noble metal nanoclusters in oxides has so far been found in catalysts; the formation of active metal nanoparticles under certain conditions (e.g., in a reducing atmosphere) is occasionally useful and is termed “intelligent catalysis” [18-19]. From the results of the present experiment, we can see the effect of platinum nanoparticle precipitation on the electrical

conductivity of a proton conductor; the changes occurred reversibly as a result. It should be noted that the platinum nanoparticles are formed uniformly in the interior of the oxide grain in the present case, thus influencing the electrical conductivity of the oxide.

Why did the conductivity decrease upon precipitation of platinum nanoparticles in the proton-conducting oxide? We must first consider a main concept of "nanoionics", namely, the formation of space charges that cause the eventual shift in the defect equilibrium, and determine whether or not this actually occurred in the present platinum-containing perovskite. Electron holography, whereby the electrostatic inner potential is measured as a change in electron-wave phase, is an effective technique for answering these questions.

Figure 5 shows the results of the electron holography and schematic illustrations of precipitated platinum nanoparticles in the proton-conducting oxide. Figure 5 (A) shows a reconstructed electron phase image at a $Pt/SrZr_{0.9}Y_{0.1}O_{3-\alpha}$ interface, and Figure 5 (B) shows the phase profile at this interface, where some phase deviations can be seen. It should be noted that the measurement was performed on a micrometer-sized platinum particle embedded in the perovskite oxide, because the present materials have very small distances between the platinum nanoparticles as shown in Figure 5 (A). The results indicate that the oxide phase is more negatively charged within the distance of approximately 25 nm from the interface (Figure 5 (B)). As mentioned above, the thickness of the space charge layer is two to several times the Debye length [20]. The Debye length is formulated as follows [21]:

$$\lambda = \left(\frac{\varepsilon_0 \varepsilon_r kT}{2Z^2 e^2 c_\infty} \right)^{\frac{1}{2}}, \qquad (1)$$

where ε_0 is the permittivity of free space, ε_r is the dielectric constant, Z is the charge number, e is the elementary charge and c_∞ is the bulk proton concentration. When we assume a dielectric constant of $\varepsilon_r = 10$ and proton concentration of 10% of the acceptor concentration at 1000 °C (i.e., $c_\infty = 1.56 \times 10^{-26}$ m^{-3} for the Y-doped $SrZrO_3$) [14], the Debye length is estimated to be about 0.4 nm. Hence, the effective thickness of the space charge layer is found to be around 2 nm and the distance of 25 nm appears to be an overestimation. This is partly because the holography measurement was conducted at room temperature and the space charge thickness typically decreases at high temperature. However, the variation in the inner potential within the $SrZr_{0.9}Y_{0.1}O_{3-\alpha}$ phase (abbreviated as SZO in Figure 5 (A) and 5(B)) reveals the occurrence of charge transfer, and the resulting formation of the space change region; the strontium zirconate

phase is negatively charged at the interface with metallic platinum. If the space change is considered to originate from the difference in work functions between the platinum and $SrZr_{0.9}Y_{0.1}O_{3-\alpha}$ phases, the work function of the oxide phase should be higher than that of platinum [15]. The work function of platinum is reported to be 5.0-5.2 eV. The work function of Y-doped $SrZrO_3$ is not available in the literature, but it must be higher than that of platinum because the oxide is a *p*-type semiconductor and the band gap is as wide as the work function of platinum [22]. Thus, the negative charge of the oxide phase is reasonable. In the specimen containing platinum nanoparticles, the size of the platinum particles is much smaller than that used in the electron holography measurements, and the amount of charge transfer may be smaller. However, the tendency of the oxide phase to become negatively charged upon coming into contact with platinum metal will not differ.

This can further explain the conductivity drop in terms of defect equilibria in a proton-conducting oxide where the amount of protons decreases in the oxide lattice in response to receiving the negative charge. $SrZr_{0.9}Y_{0.1}O_{3-\alpha}$ is designed to have oxygen vacancies by substitution of Y^{3+} for Zr^{4+} of the original composition $SrZrO_3$, where α denotes the amount of oxygen vacancy in the compound. In oxidative atmospheres, excess oxygen enters the oxygen vacancies leading to a generation of electron holes according to the following equilibrium:

$$V_{O}^{\bullet\bullet} + \frac{1}{2}O_2 \rightleftarrows O_{O}^{x} + 2h^{\bullet}, \qquad (2)$$

where $V_{O}^{\bullet\bullet}$, O_{O}^{x}, $h^{\bullet}$ and $H_{i}^{\bullet}$ represent an oxygen vacancy, a lattice oxygen, a hole and a proton, respectively, using Kröger-Vink notation. Holes and protons are in an equilibrium expressed by the following equation:

$$H_2O + 2h^{\bullet} \rightleftarrows 2H_{i}^{\bullet} + \frac{1}{2}O_2. \qquad (3)$$

Furthermore, the chemical equilibrium of water formation can be written as follows:

$$H_2 + \frac{1}{2}O_2 \rightleftarrows H_2O. \qquad (4)$$

Thus, combining Eq. (3) and Eq. (4) yields

$$H_2 + 2h^{\bullet} \rightleftarrows 2H_{i}^{\bullet}. \qquad (5)$$

Finally, electrons and holes are in equilibrium in the band structure of the oxide:

$$e' + h^{\bullet} \rightleftarrows \text{Nil}. \qquad (6)$$

When $SrZr_{0.9}Y_{0.1}O_{3-\alpha}$ is negatively charged at the interface with platinum, the concentration of electrons is assumed to increase and the number of holes is assumed to decrease in accordance with the equilibrium in Eq. (6). Following the decrease in the hole concentration, Eq. (5) suggests a consequent decrease in the concentration of protons at a given partial pressure of hydrogen. Therefore, it can be thought that proton and hole concentrations decrease for the negatively charged space charge layer in the oxide, that is, the amount of protons and holes decrease in the oxide lattice in response to the negative charge. Thus, the experimental results presented here support the formation of negative charge at the interface with platinum, and explain the decrease in proton conductivity for the perovskite containing platinum nanoparticles.

It will be important to examine the effects of varying the amount of platinum and the temperatures during hydrogen exposure, and many factors still remain to be investigated. Although the nanoionics effect demonstrated in this study was unfortunately decreased ion conductivity, it was interesting to observe the reversible nanoionics phenomenon in the blue platinum-containing perovskite (Figure 2), and to find that only a small amount of platinum can significantly alter the proton conductivity of an oxide through a nanoionics phenomenon.

4. Conclusions

In this report, a nanoionics phenomenon in a Pt-containing proton-conducting oxide ($Pt/SrZr_{0.9}Y_{0.1}O_{3-\alpha}$) was demonstrated. The platinum phase was introduced to the material by a combustion synthesis method followed by sintering at a controlled temperature, successfully forming a solid solution of platinum in the perovskite lattice. The nanoionics phenomenon occurred reversibly in response to the precipitation and solid dissolution of platinum nanoparticles under reducing and oxidizing ambient atmospheres, respectively. When the blue perovskite containing a solid-solved platinum phase was exposed to a hydrogen atmosphere at 1000 °C, the electrical conductivity dropped significantly and the color of the specimen changed to black. The results of XAFS measurements, TEM analysis, and electron holography revealed that platinum nanoparticles precipitated homogenously in the oxide and an uneven distribution of negative and positive space charges formed at the interface between the oxide and platinum. These precipitates disappeared upon exposure of the specimen to an oxidizing atmosphere, and conductivity recovered accordingly. The phenomenon observed in the blue perovskite provides

evidence of the nanoionics effect; in other words, a very small amount of precipitated platinum nanoparticles markedly changed the ion-conducting properties of the perovskite oxide.

Acknowledgements

This study was supported by a Grant-in-Aid for Scientific Research on Priority Areas "Nanoionics (No. 439)" from the Ministry of Education, Culture, Sports, Science and Technology of Japan. XAFS spectra were measured at Photon Factory, High Energy Accelerator Research Organization, KEK, in Tsukuba, Japan.

References

1. H. Rickert, *Inorganic Chemistry Concepts 7* (1982), 118.
2. T. Kudo and K. Fueki, *Solid Stale Ionics* (1990).
3. S. Bredikhin, T. Hattori and M. Ishigame, *Physical Review B* **50** (1994) 2444.
4. J. Maier, *Solid State Ionics* **143** (2001) 17.
5. J. Schoonman, *Solid State Ionics* **157** (2003) 319.
6. J. Maier, *Nature Materials* **4** (2005) 805.
7. C.C. Liang, *Journal of the Electrochemical Society* **120** (1973) 1289.
8. I. Kosacki, T. Suzuki, V. Petrovsky and H.U. Anderson, *Solid State Ionics* **136-137** (2000) 1225.
9. N. Sata, K. Eberman, K. Eberl and J. Maier, *Nature* **408** (2000) 946.
10. N. Ito, M. Iijima, K. Kimura and S. Iguchi, *Journal of Power Sources* **152** (2005) 200.
11. S. Tao and J.T.S. Irvine, *Advanced Materials* **18** (2006) 1581.
12. H. Iwahara, T. Esaka, H. Uchida and N. Maeda, *Solid State Ionics* **3-4** (1981) 359.
13. T. Norby, *Solid State Ionics* **125** (1999) 1.
14. K.D. Kreuer, *Annual Review of Materials Research* **33** (2003) 333.
15. H. Matsumoto, Y. Furya, S. Okada, T. Tanji and T. Ishihara, *Electrochemical and Solid-State Letters* **10** (2007) P11.
16. H. Matsumoto, Y. Furuya, S. Okada, T. Tanji and T. Ishihara, *Science and Technology of Advanced Materials* **8** (2007) 531.
17. T. L. Nguyen, M. Dokiya, S. Wang, H. Tagawa and T. Hashimoto, Solid State Ionics, **130**

(2000) 229.

18. Y. Nishihata, J. Mizuki, T. Akao, H. Tanaka, M. Uenishi, M. Kimura, T. Okamoto and N. Hamada, *Nature* **418** (2002) 164.

19. M. Taniguchi, H. Tanaka, M. Uenishi, I. Tan, Y. Nishihata, J. Mizuki, H. Suzuki, K. Narita, A. Hirai and M. Kimura, *Topics in Catalysis* **42-43** (2007) 367.

20. S. Kim and J. Maier, *J. Electrochem. Soc.* 149 (2002), J 73.

21. S. J. Litzelman, J. l. Hertz, W. Jung and H. L. Tuller, *Fuel Cells* **8** (2008) 294.

22. T. Higuchi, H. Matsumoto, T. Shimura, K. Yashiro, T. Kawada, J. Mizusaki, S. Shin and T. Tsukamoto, *Jpn. J. Appl. Phys., Part 1* **43** (2004) 5419.

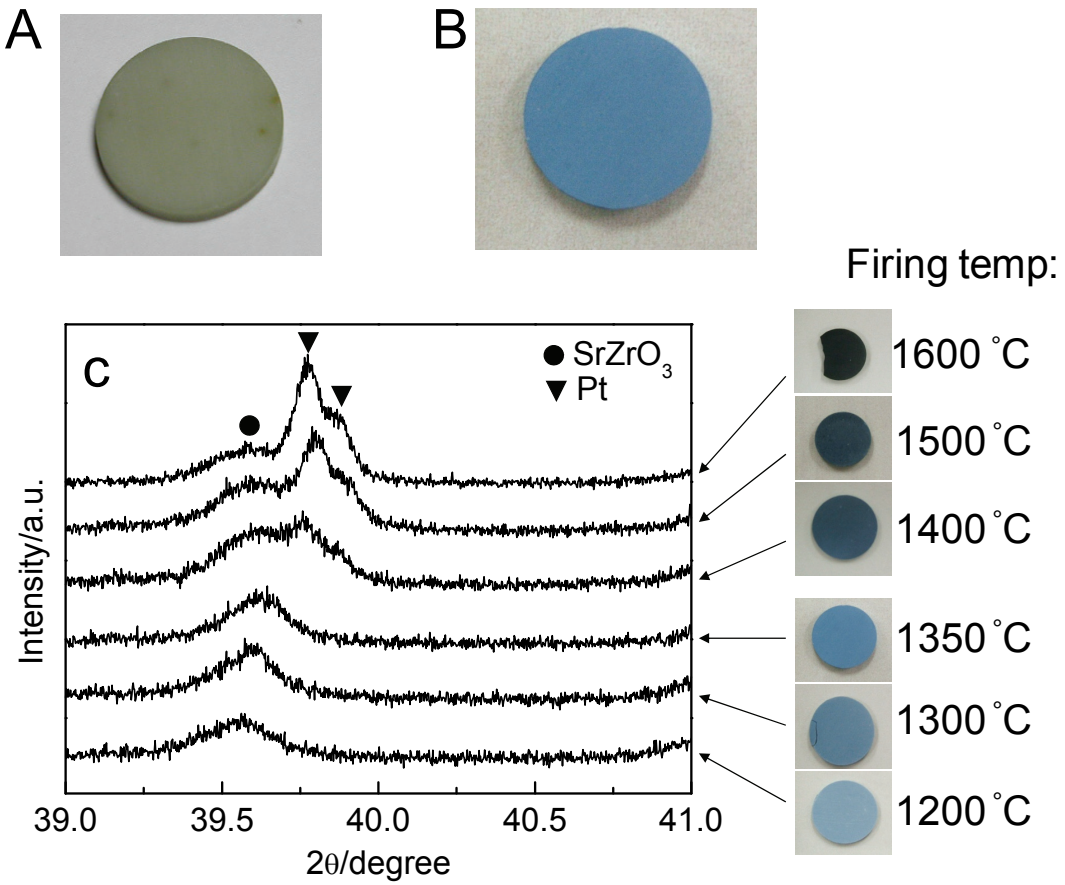

Figure 1. Appearances of (A) $SrZr_{0.9}Y_{0.1}O_{3-\alpha}$ (platinum free, sintered at 1600°C); (B) Pt-containing $SrZr_{0.9}Y_{0.1}O_{3-\alpha}$ (as sintered at 1350°C); and (C) the XRD patterns of Pt-containing $SrZr_{0.9}Y_{0.1}O_{3-\alpha}$ sintered at different temperatures and their corresponding appearances.

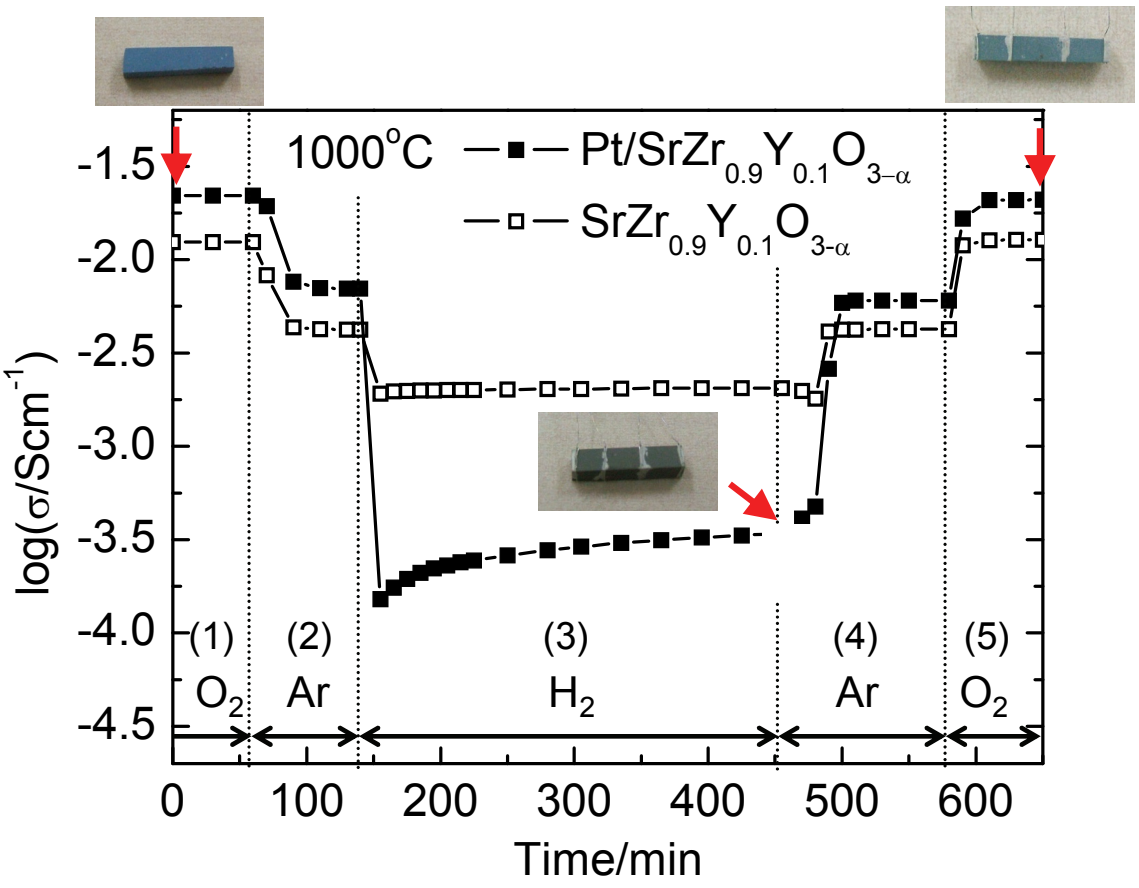

Figure 2. Electrical conductivity of $SrZr_{0.9}Y_{0.1}O_{3-\alpha}$ and Pt-containing $SrZr_{0.9}Y_{0.1}O_{3-\alpha}$ at 1000°C in a succession of different ambient atmospheres.

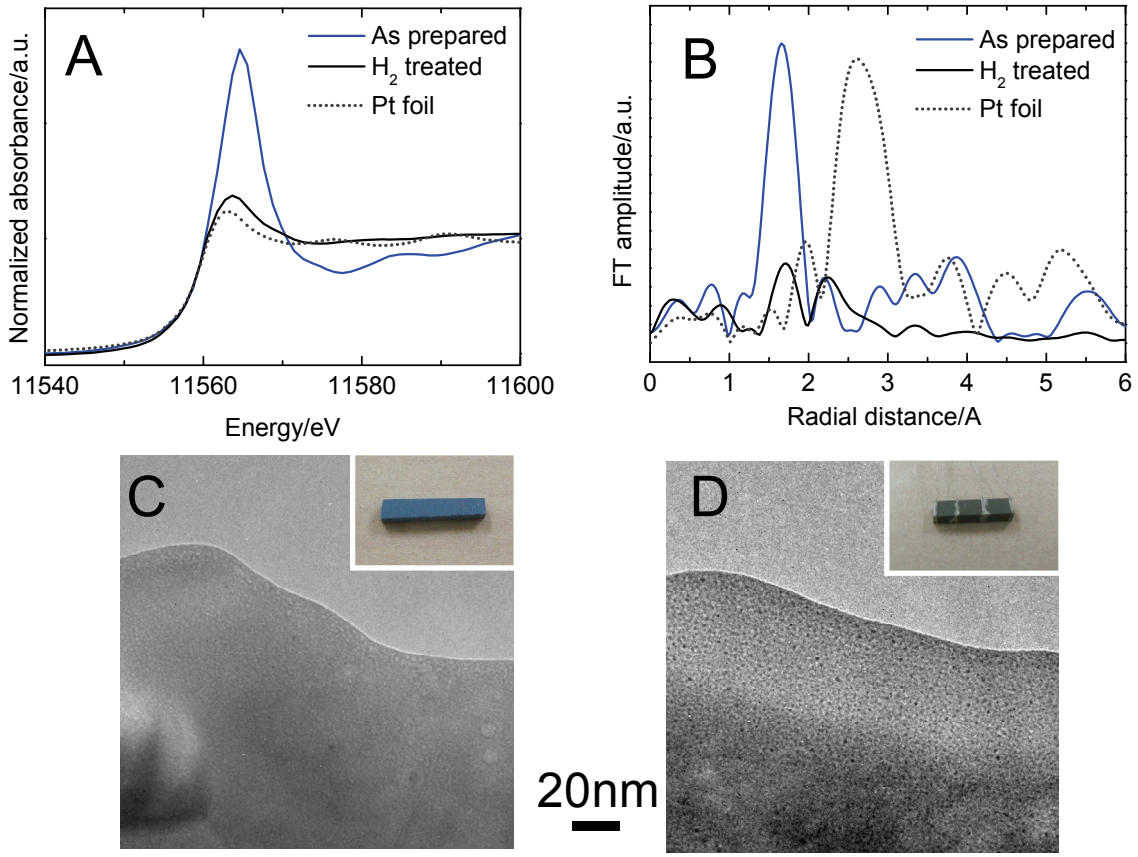

Figure 3. Results of XAFS measurement and TEM images of as-prepared (blue) and hydrogen-treated (black) Pt-containing samples. (A) Normalized Pt L_{III}-edge XANES spectra; (B) radial structural functions around a platinum atom obtained from the Pt L_{III}-edge EXAFS oscillation; and TEM images of (C) as-prepared (blue) and (D) hydrogen-treated (black) Pt-containing samples (with a 20-nm scale bar).

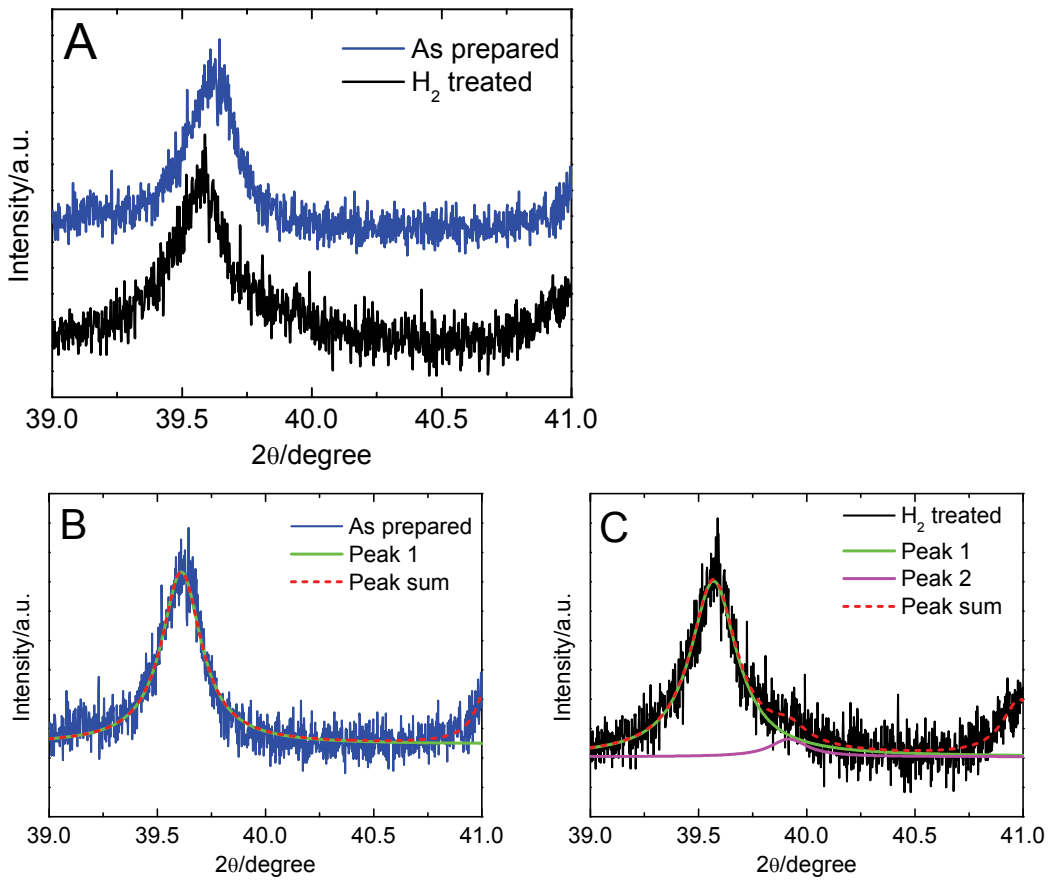

Figure 4. X-ray diffraction patterns of Pt-containing $SrZr_{0.9}Y_{0.1}O_{3-\alpha}$ sintered at 1350°C, before and after hydrogen exposure at 1000°C. In B and C, the patterns were peak-deconvoluted by Lorentz curves.

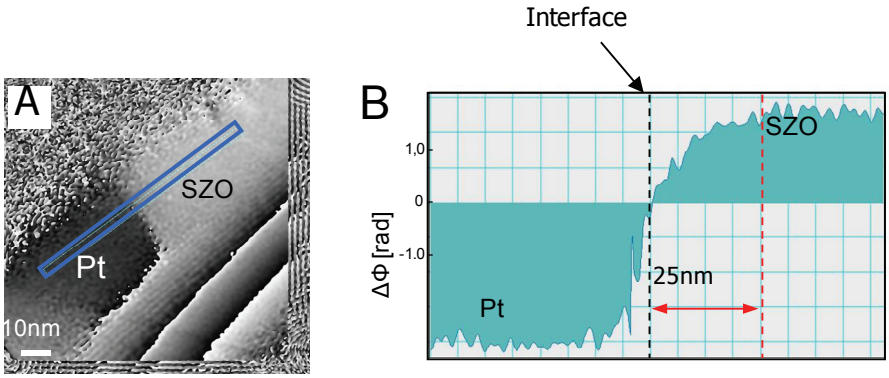

Figure 5. Results of the electron holography and schematic illustrations of platinum nanoprecipitates in the proton-conducting oxide: (A) Reconstructed electron phase image at a Pt/$SrZr_{0.9}Y_{0.1}O_{3-\alpha}$ interface; (B) Phase profile along the long side of the blue rectangle in (A) averaged over the width.